IOP Publishing Superconductor Science and Technology
Supercond. Sci. Technol. 31 (2018) 015020 (9pp) https://doi.org/10.1088/1361-6668/aa9b1e

Superconductivity and valence state in layered single-crystal $HfAs_{1.67}Te_{0.12}$

Jian Peng[1,2], Jia Yu[1,3], Shuai Zhang[1] and Genfu Chen[1,3,4]

[1] Beijing National Laboratory for Condensed Matter Physics, and Institute of Physics, Chinese Academy of Sciences, Beijing 100190, People's Republic of China
[2] Department of Physics, Beijing Jiaotong University, Beijing 100044, People's Republic of China
[3] University of Chinese Academy of Science, Beijing 100049, People's Republic of China
[4] Collaborative Innovation Center of Quantum Matter, Beijing 100190, People's Republic of China

E-mail: szhang@iphy.ac.cn and gfchen@iphy.ac.cn

Received 27 September 2017, revised 13 November 2017
Accepted for publication 16 November 2017
Published 13 December 2017

Abstract

We report a detailed study on single crystals of $HfAs_{1.67}Te_{0.12}$ within a PbFCl-type layered structure. The single crystals of the title compound were successfully grown using a chemical transport reaction. The temperature dependence of electrical resistivity $\rho(T)$, AC magnetic susceptibility $\chi_{AC}(T)$ and specific heat $C(T)$ show a bulk superconductivity with transition temperature $T_c = 1.67$ K. The jump of C/T at T_c is comparable to the traditional BCS weak-coupling model. A full H–T phase diagram is established using the results of $\rho(T, H)$ and $C(T)$ under fields, suggesting a rather weak anisotropy $[(H_{c2}^{\parallel ab}(0)/H_{c2}^{\parallel c}(0)]$ of 1.8 in orbital limit dominated three-dimension-like superconducting system. The mixed-valence states of Hf and As observed in the binding energy from x-ray photoelectron spectroscopy are consistent with the single-crystal x-ray diffraction analysis, indicating that the As–Te disorder prefers to occur in the [HfAs] layer and a large amount of vacancies are present in tetragonal As layer. As compared to $HfAs_{1.7}Se_{0.2}$ ($T_c = 0.52$ K), a positive-like vacancy effect on T_c has been confirmed in $HfAs_{1.67}Te_{0.12}$. The analysis of the Hall coefficient implies that the hole-type carriers dominate the transport properties, which is in good agreement with the hole pockets at Fermi surface obtained in a band structure calculation. The detailed study of single-crystal $HfAs_{1.67}Te_{0.12}$ provides a possible candidate to discuss the non-magnetic Kondo effect.

Keywords: superconductivity, $HfAs_{1.67}Te_{0.12}$, valence state, vacancy defect, PbFCl-type

(Some figures may appear in colour only in the online journal)

1. Introduction

Lots of exciting phenomena including high-T_c superconductors and topological materials have been found to be related to the character of d electrons in transition metals, especially within a low-dimension structure, which has been considered as a key factor for underlying superconductivity. In systems with single d electron, previous studies already discovered some remarkable superconductors such as $LiTi_2O_4$ [1], Cu_xTiSe_2 [2] and carrier-doped MNCl (M: Ti, Zr, and Hf) [3–5]. Recently, intense research interests have been attracted on another ternary pnictide-chalcogenides APn_{2-x} Ch_x system (A: Zr, Hf; Pn: P, As; Ch: S, Se) [6–9] within PbFCl-type layered structure, which is the same as that of '111' iron-based superconductor family. Although this composition appears to be a substitution system, the binary composition with none and full substitution at Pn sites such as APn_2 and ACh_2 can crystallize only in $PbCl_2$-[10] and CdI_2-type structure, [11] respectively, which are completely different from the ternary phase. In the series of AP_{2-x} Ch_x (A: Zr, Hf; Ch: S, Se), [9] all combinations show superconductivity with a dome-like phase diagram, and the highest value of $T_c = 6.3$ K was found in $ZrP_{1.25}$ $Se_{0.75}$. In contrast, only $HfAs_{1.7}$ $Se_{0.2}$ [12] has been found to be superconductor with $T_c = 0.52$ K in the series of AAs_{2-x} Ch_x (A: Zr, Hf; Ch: Se, Te). In a very recent study, [13] more interestingly, a non-magnetic two-channel Kondo effect (2CK) was proposed to explain the abnormal $-|A|T^{1/2}$

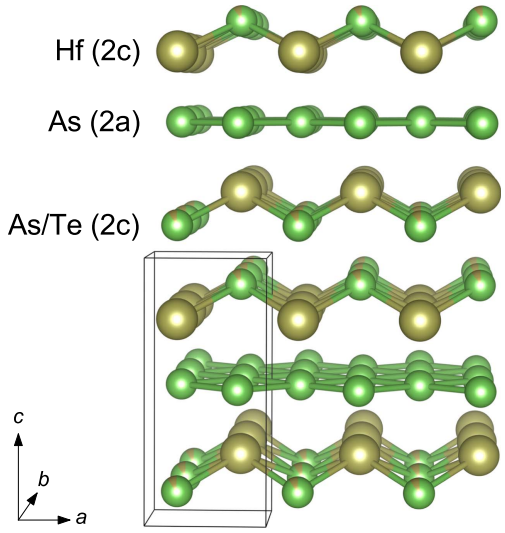

Figure 1. Schematic illustration of the PbFCl-type $HfAs_{1.67}Te_{0.12}$.

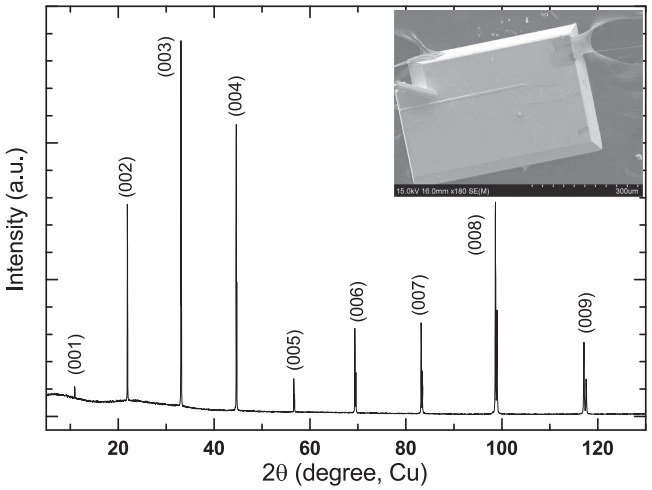

Figure 2. Single-crystal diffraction pattern of $HfAs_{1.67}Te_{0.12}$ with only (00*l*) diffraction peaks. The inset shows the SEM image of a typical plate-shape single crystal.

term observed in the low-temperature resistivity of $ZrAs_{1.58}Se_{0.39}$. The 2CK effect seems to originate from a dynamic Jahn–Teller effect operating at the vacancy-carrying As layer, which is also responsible for the low superconducting (SC) transition temperature $T_c = 0.14$ K as compared with the free-of-vacancies homologue $ZrP_{1.54}S_{0.46}$ with $T_c = 3.7$ K.

In terms of structure feature, pnictide (Pn: P, As) occupies two inequivalent sites (2*a* and 2*c*) in PbFCl-type structure as shown in figure 1. Although the assumption of disordered Si and As occupying the 2*a* site was employed for $HfAs_{2-x}Si_x$ [14], a number of firm experimental facts and structure analysis imply that the random substitution of Pn with Ch prefers to occur only in 2*c* site. In the case of APn_xCh_y with $1 < x + y < 2$, it is of importance to determine whether the vacancies are exactly present in the Pn layers (2*a* site) and how the vacancies affect the properties. On the other hand, the anions in PbFCl-type compounds appear to form a polyanionic Pn–Pn bonding suggesting a covalent character. Correspondingly, the large amount of vacancies can alter the physical properties by directly influencing the valence state.

In this paper, thus, we report a detailed study on another new member of the ternary $APn_{2-x}Ch_x$ family, $HfAs_{1.67}Te_{0.12}$, crystallizing in PbFCl-type structure with a large number of vacancies in As–As layers. The bulk superconductivity with $T_c = 1.67$ K has been confirmed in electrical resistivity, AC magnetic susceptibility and specific heat. The hole-type carriers dominated transport properties are consistent with the Fermi pockets found at Fermi level in a band structure calculation.

2. Experimental details

High-quality single crystals of $HfAs_{1.67}Te_{0.12}$ with typical dimensions $0.5 \times 0.4 \times 0.1$ mm^3 were grown using a chemical transport method, in which the iodine was used as transport agent in a temperature gradient from 1123 (sink) to 1223 K (source). The structure and chemical composition of $HfAs_{1.67}Te_{0.12}$ crystals were determined using powder and single-crystal x-ray diffraction pattern, Thermo IRIS Intrepid II inductively coupled plasma (ICP), and Oxford X-Max energy disperive x-ray spectroscopy (EDX), which are consistent with each other and reveal that the title compound crystallizes in a PbFCl-type structure (sapce group $P4/nmm$, No. 129), as shown in figure 1. The electrical resistivity under different magnetic fields was measured using a conventional four-probe method with magnetic field always perpendicular to the flowing current. A dozen single crystals were used to gain sufficient mass for the measurement of specific heat, which was measured by a relaxation technique. Measurement of AC magnetic susceptibility was carried out using a homemade coil on the dilution option of physical property measurement system (PPMS Quantum Design). The x-ray photoelectron spectroscopy (XPS) measurements were performed on a Thermo Scientific ESCALAB 250X spectometer fitted with a monochromatic Al K_α x-ray source. The binding energy (BE) was measured on plate-shape single crystals with area as small as $\sim 500 \times 400$ μm^2. Electronic band structure was calculated using the program CASTEP with the local-density-approximation with CA-PZ function; a $54 \times 54 \times 25$ Monkhorst Pack mesh was used for *k*-point sampling with the Brillouin Zone of the tetragonal unit cell.

3. Results and discussion

The powder x-ray diffraction (XRD) pattern obtained by grinding lots of single crystals (not shown here) is indexed on the basis of a tetragonal unit cell with $a = b = 3.6695(5)$ Å and $c = 8.1395(5)$ Å. Figure 2 displays a typical XRD patterns observed on single-crystal $HfAs_{1.67}Te_{0.12}$. Note that the appearance of only (00*l*) diffraction peaks suggests the crystal growth along the *ab* plane and stacking in *c* direction. The EDX results indicate that the average Hf:As+Te atomic

Table 1. Crystallographic data and details of the structure determination for $HfAs_{1.67}Te_{0.12}$.

Empirical formular	$HfAs_{1.68}Te_{0.09}$
Formula weight [g mol^{-1}]	315.905
Temperature [K]	293
Radiation wavelength [Å]	0.71073
Crystal size [mm^3]	0.097 × 0.430 × 0.513
Space group	$P4/nmm$ (No. 129)
Unit cell dimensions	
$a(=b)$ [Å]	3.6758(2)
c [Å]	8.1259(5)
Volume [Å^3]	109.793(14)
Formula unit per cell	2
Calculated density [g cm^{-3}]	9.55
Absorption coefficient [mm^{-1}]	73.3
Measurement range in θ [deg]	2.51–27.86
Index ranges	$-4 \leqslant h, k \leqslant 4$
	$-10 \leqslant l \leqslant 10$
Transmission factors	0.003–0.029
Reflection collected	361
Independent reflections	106 ($R_{int} = 0.0899$)
Structure solution program	XT, Ver. 2014/4
Refinement method	Full-matrix
	least-squares on F^2
Refinement program	SHELXL-2014/7
Extinction coefficient	0.0250(30)
Data/restraints/parameters	91/0/11
Goodness-of-fit on F^2	1.339
Final R indices (all F_o)	$R_1 = 0.0470$, $W R_2 = 0.1089$

ratio is approximately 1:1.8, which is in good agreement with the ICP result 1:1.67:0.12. All the physical properties were measured on the high-quality-plate-shape single crystal, as shown in the inset of figure 2.

To the best of our knowledge, this is the first detailed report of Hf–As–Te ternary phase with PbFCl-type structure. Thus, the single-crystal XRD analysis was performed to study the crystallographic data, which are summarized in tables 1 and 2. In our analysis results, As occupies two inequivalent sites of 2*b* and 2*c*, in which the 2*b* is equivalent to the 2*a* corresponding different definition of coordinate. Both the EDX and ICP yield a quite low concentration of As+Te, indicating a large amount of vacancies in the system. Several arragnements of the Te occupation have been tried in single-crystal XRD analysis. It appears that the substitution of As with Te prefers to occur in Hf–As layer (2*c* site), leading to near 0.21 vacancy per formula composition in tetragonal As–As layer (2*b*). In comparison with previous reports of the $APn_{2-x}Ch_x$ [6–9, 13], the present system shows the heaviest mole mass, the lowest substitution level and the largest amount of vacancies.

The temperature dependence of electrical resistivity $\rho(T)$ between 300 K and 50 mK is shown in figure 3. The metallic characteristic with a linear-like $\rho(T)$ above ~50 K and constant value below 20 K are confirmed in all examined single crystals. Note that the residual resistivity ratio (RRR = $\rho_{300\,K}/\rho_{2K}$) appears to be as low as 1.5, which might be acceptable for polycrystalline samples with more boundary

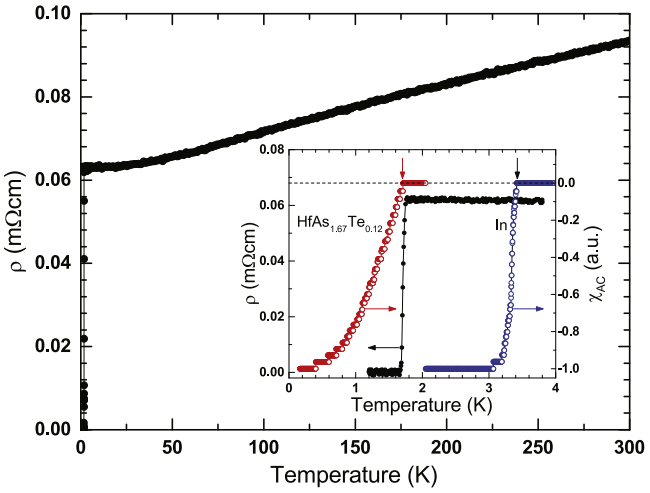

Figure 3. Temperature dependence of electrical resistivity $\rho(T)$. The inset shows $\rho(T)$ (left scale) and AC magnetic susceptibility $\chi_{AC}(T)$ (right scale) at temperatures lower than 4 K. Pure indium (In) was used as a reference in $\chi_{AC}(T)$ measurement.

scattering effect, but rather strange for high-quality single crystals as studied in the present system. In the meanwhile, such a temperature dependence has already been observed in all the polycrystalline and single-crystal samples of the $APn_{2-x}Ch_x$ system [6–9]. Thus, we consider that the low RRR could be intrinsic and caused by a combination effect of the disorder substitution in [HfAs] layer and the vacancies scattering in As–As layer, which could be more significant because of the large number of vacancies confirmed in the present system.

As shown in the inset of figure 3, a sharp drop corresponding to the SC transition is present at 1.67 K in $\rho(T)$ of $HfAs_{1.67}Te_{0.12}$. The 10%–90% width, $W_{10\%-90\%}$, of the SC transition in zero field is 0.04 K, implying again the considerably high quality of the crystals used in the present study. In the meanwhile, the SC transition can also be confirmed in AC magnetic susceptibility $\chi_{AC}(T)$, which displays an apparent drop around 1.7 K with $T_c = 3.4$ K confirmed in $\chi_{AC}(T)$ of the reference material indium, as shown in the inset of figure 3. Upon the comparison with normalized $\chi_{AC}(T)$ of In, the SC volume fraction is estimated to be close to 100% by ignoring the demagnetization effect. Based on the analysis of the SC transition in $\rho(T)$ and $\chi_{AC}(T)$, we reasonably conclude that $HfAs_{1.67}Te_{0.12}$ shows bulk superconductivity with $T_c = 1.67$ K, as also confirmed in specific heat $C/T(T)$.

The directions of *a* and *b*, identical in the PbFCl-type structure, are used to describe the configuration of magnetic field and current directions. To study the SC phase of the title compound, $\rho(T)$ with flowing current $I \| b$ was measured under magnetic fields with $H \| c$ and $H \| a$ crystallographic axes, as shown in figures 4(a) and (b), respectively. As applying field $H \| c$, other than the monotonic suppression of the T_c, a two-step anomaly becomes more obvious in fields. To quantitatively evaluate the shift of T_c observed in $\rho(T)$ under H, T_c is defined as the temperature where $\rho(T)$ reaches zero resistance. T_c decreases monotonically from 1.67 to 0.39 K with increasing H up to 0.26 T in a step of 0.2 T, and fields higher

Table 2. Wyckoff positions (W.p.), atomic coordinates and coefficients U_{ij}(Å^{-2}) of the anisotropic displacement parameters according to $-2\Pi^2[h^2a^{*2}U_{11} + \cdots + 2hka^*b^*U_{12}]$ for $HfAs_{1.67}Te_{0.12}$. U_{eq} is defined as 1/3 of the trace of the orthogonalized U_{ij} tensor.

Atom	W.p.	x	y	z	Occ.	$U_{11} = U_{22}$	U_{33}
Hf01	2*c*	1/4	1/4	0.2350(1)	1	0.0188(9)	0.0126(11)
As02	2*b*	3/4	1/4	1/2	0.76	0.0245(12)	0.0115(19)
As03	2*c*	3/4	3/4	0.1166(3)	0.91	0.0183(11)	0.0139(18)
Te04	2*c*	3/4	3/4	0.1166(3)	0.09	0.0183(11)	0.0139(18)

Note. $U_{12} = U_{13} = U_{23} = 0$

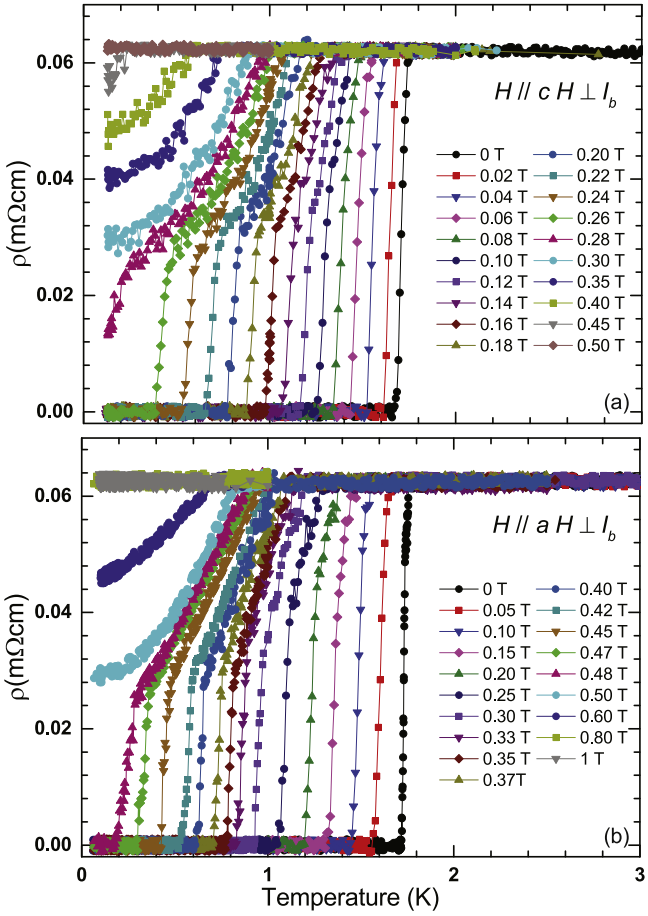

Figure 4. Temperature dependence of resistivity $\rho(T)$ under fields with $H\|c$ (a) and $H\|a$ (b). The current orientation is always parallel to b.

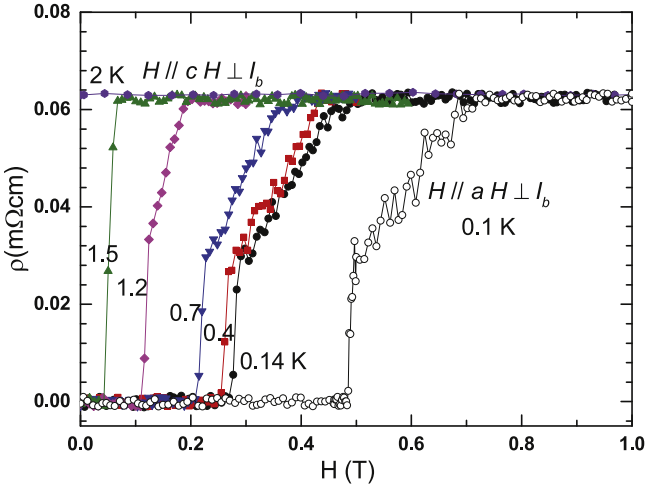

Figure 5. Isothermal field dependence of resistivity with $H\|c$ at 0.14, 0.4, 0.7, 1.2, 1.5 K and $H\|a$ at 0.1 K. The current orientation is always parallel to b.

than 0.5 T force the $\rho(T)$ back to the value of normal-state resistivity ρ_{normal} without obvious temperature dependence. The transition close to the onset becomes broader and quadratic with increasing H, whereas the other is rather sharp in whole field region. Similar phenomena have also been confirmed in the configuration of $H\|a$, as shown in figure 4(b). More importantly, the broadened transition close to the onset show a clear anisotropy, which is similar to the determined T_c.

Although there is no signature of the two-step transition in zero field, we prefer to consider the two-step transition to be a result of phase separation rather than some kind of field induced anomaly. Firstly, with increasing field, the onset of the transition in $\rho(T)$ and T_c shift to lower temperatures at a similar rate, strongly implying that both the two phases are related to superconductivity. Secondly, the two-step transition show a similar anisotropy compared to the anisotropy found for T_c. Finally, the broadened transition could be related to additional scattering effect caused by the flux motion.

To double-check the SC phase under fields, we measured the isothermal magnetic field dependence of resistivity $\rho(H)$ with $H\|c$ and $H\|a$, as shown in figure 5. With increasing H, $\rho(H)$ at 0.14, 0.4, 0.7 and 1.2 K show a sharp upturn followed by a smooth linear increase up to the normal-state resistivity. Note that the two-step transition is rather weak as the temperature is close to the T_c at zero field (e.g. 1.5 K). At temperature higher than T_c such as 2 K, $\rho(H)$ shows no obvious field dependence. In the meanwhile, $\rho(H)$ at 0.1 K with $H\|a$ shows the same two-step transition as already observed in $\rho(T)$. The tendency of $\rho(H)$ is the same as that of $\rho(T)$, which suggests again that the two-step transition of resistivity under fields is not extrinsic but intrinsic nature. To keep consistent with the definition of T_c, the H_{c2} at different temperature is defined as the field where $\rho(H)$ reaches zero resistance. All the T_cs at different H and H_{c2}s at different temperatures are used to establish a SC phase diagram.

The superconductivity is also studied by measuring the temperature dependence of specific heat $C(T)$ under fields. As shown in figure 6, $C/T(T)$ in zero field shows a sharp jump at $T_c = 1.67$ K, as determined using an *isoentropic* method in the inset. The ΔC at T_c is found to be 8.02 mJ mol^{-1} K^{-1}, which is slightly less than the expected value of the BCS

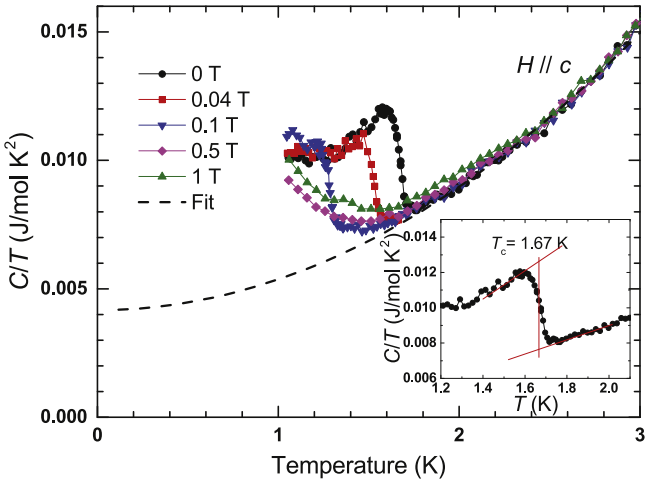

Figure 6. Temperature dependence of C/T in fields with $H\|c$. The dashed line represents the fitting of C/T at high temperatures ($T \geqslant 2$ K). The inset shows the isoentropic method used to determine T_c.

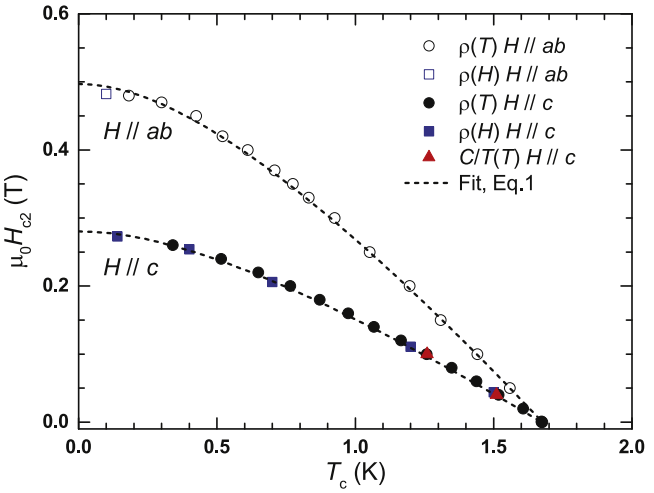

Figure 7. $H-T$ phase diagram summarized from $\rho(T, H)$ and $C/T(T)$. The dotted lines are fittings of the data with WHHM model without considering spin–orbital coupling contribution (λ).

theory ($\Delta C_{el}/\gamma_n T_c \sim 1.43$) for a weakly coupled single-band s-wave superconductor. Note that such a sharp jump at T_c is consistent with the SC transition found in $\rho(T)$ and $\chi_{ac}(T)$, proving again the bulk superconductivity observed in single-crystal $HfAs_{1.67}Te_{0.12}$. A fit of the normal state ($T \geqslant 2$ K) $C(T)$ with $C = \gamma_n T + \beta T^3$ gives $\gamma_n = 4.0$ mJ mol^{-1} K^{-2} and $\beta = 1.3$ mJ mol^{-1} K^{-4} shown as a dashed line in figure 6. With increasing fields with $H\|c$, T_c shifts to lower temperatures without obvious weakening of the SC jump. As increasing H up to 0.5 and 1 T, SC transition disappears and $C/T(T)$ turns to be a smooth tail. The field dependence of T_c observed in $C/T(T)$ shows a great agreement with those confirmed in $\rho(T)$ under fields. Thus, such an enhancement of $C/T(T)$ caused by high fields could be intrinsic. However, due to mechanical problem of our DR option of PPMS, the reliable $C(T)$ cannot be measured stably below 1 K.

The resulting H–T phase diagram obtained from $C/T(T)$ under fields with $H\|c$ and $\rho(T, H)$ with $H\|c$ and $H\|a$ is shown in figure 7. The upper critical field H_{c2}(T) is fitted using a single-band Werthamer–Helfand–Hobenberg–Maki (WHHM) method described as equation (1), which includes the effects of Pauli spin paramagnetism, spin–orbit scattering, and orbital diamagnetic effects.

$$\ln\frac{1}{t} = \left(\frac{1}{2} + \frac{i\lambda_{so}}{4\gamma}\right)\psi\left(\frac{1}{2} + \frac{h + \frac{1}{2}\lambda_{so} + i\gamma}{2t}\right) + \left(\frac{1}{2} - \frac{i\lambda_{so}}{4\gamma}\right)\psi\left(\frac{1}{2} + \frac{h + \frac{1}{2}\lambda_{so} - i\gamma}{2t}\right) - \psi\left(\frac{1}{2}\right), \quad (1)$$

where $t = T/T_c$, $h = 4H_{c2}/[-\pi^2 T_c (dH_{c2}/dT)_{T=T_c}]$, $\gamma = \left[(\alpha h)^2 - \left(\frac{1}{2}\lambda_{so}\right)^2\right]^{0.5}$, and ψ is digamma function. α and λ_{so} represent the spin paramagnetic (Maki parameter [15, 16]) and spin–orbit scattering effects, respectively. $\alpha = \sqrt{2}H_{c2}^{orb}(0)/H_{c2}^{pm}(0)$ accounts for the relative contribution of orbital effect and Pauli spin paramagnetism. To simplify the fitting, we ignore the effect of spin–orbit coupling (λ_{so}). As shown in figure 7, the fits of the data with equation (1) (dotted line) yield $\alpha = 0$ for $H\|a$ and $H\|c$, implying that the orbital limit dominates in both field directions.

Another simple way to discuss the the orbital limit and Pauli paramagnetic limit at zero temperature is as follows. The $H_{c2}^{orb}(0)$ and $H_{c2}^{pm}(0)$ in dirty limit can be estimated using $H_{c2}^{orb}(0) = -0.69T_c(dH/dT)_{T=T_c}$ and $H_{c2}^{pm}(0) = 1.84T_c$. Using the T_c and dH/dT values obtained in two directions, $H_{c2}^{orb}(0)$ is calculated to be 0.28 and 0.50 T for $H\|c$ and $H\|a$, respectively, which are much less than $H_{c2}^{pm}(0) = 3.07$ T. Notice the excellent agreement between H_{c2} and the fittings. Thus, in summary, the domination of orbital limit in two field directions may suggest a 3D-like superconductivity, although the anisotropic relation $H_{c2}^{\|a}/H_{c2}^{\|c}(0)$ is calculated as 1.8 for layered $HfAs_{1.67}Te_{0.12}$. The coherence lengths (ξ_{ab} and ξ_c) can be roughly determined using the anistropic Ginzburg–Landau relation [17], $H_{c2}^{\|ab}(0) = \phi_0/(2\pi\xi_{ab}\xi_c)$ and $H_{c2}^{\|c}(0) = \phi_0/(2\pi\xi_{ab}^2)$, [18] which yield $\xi_{ab} = 342$ Å and $\xi_c = 194$ Å.

To discuss the correlation between valence state and physical properties, the valence state of Hf, As and Te has been studied in detail using XPS. The Hf 4f spectra of $HfAs_{1.67}Te_{0.12}$ are shown in figure 8. The spectra can be fitted as two doublets according to the spin–orbit splitting into the $4f_{7/2}$ and $4f_{5/2}$. The BE corresponding the possible Hf–As bond in this crystal is located at 16.7 and 18.6 eV in the high-energy part, and 14.4 and 16.1 eV in the low-energy part for $Hf_{4f7/2}$ and $Hf_{4f5/2}$, respectively. Note that the difference of BE between $Hf_{4f7/2}$ and $Hf_{4f5/2}$ is ~1.7 eV for both low- and high-energy part, which is the same of the characteristic energy separation between $Hf_{4f7/2}$ and $Hf_{4f5/2}$ states. To evaluate the valence state, we compare the BE observed in $HfAs_{1.67}Te_{0.12}$ with those of the reference compounds HfO_2 (4+) and HfN (3+). The measured BE of $Hf_{4f7/2}$ and $Hf_{4f5/2}$ for HfO_2 is 16.7 and 18.5 eV, respectively. The other two

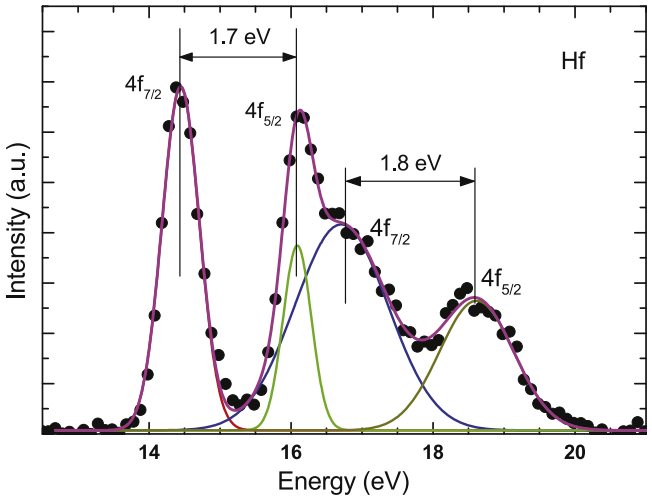

Figure 8. XPS spectra of Hf 4*f* observed on single-crystal $HfAs_{1.67}Te_{0.12}$.

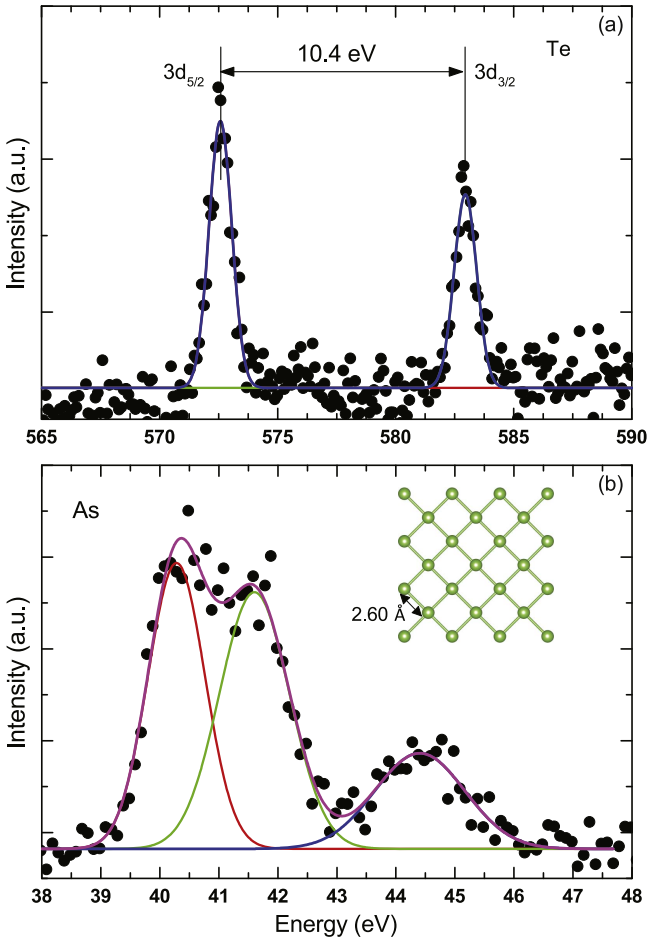

Figure 9. XPS spectra of Te3*d* (a) and As3*d* (b) observed on single-crystal $HfAs_{1.67}Te_{0.12}$. The inset shows a tetragonal As layer.

peaks around low-energy part locate slightly less than the BE of HfN with 14.9 and 16.7 eV for $Hf_{4f7/2}$ and $Hf_{4f5/2}$ states, respectively. The slight shift of BE to a lower energy in $HfAs_{1.67}Te_{0.12}$ could indicate the presence of mixed-valence

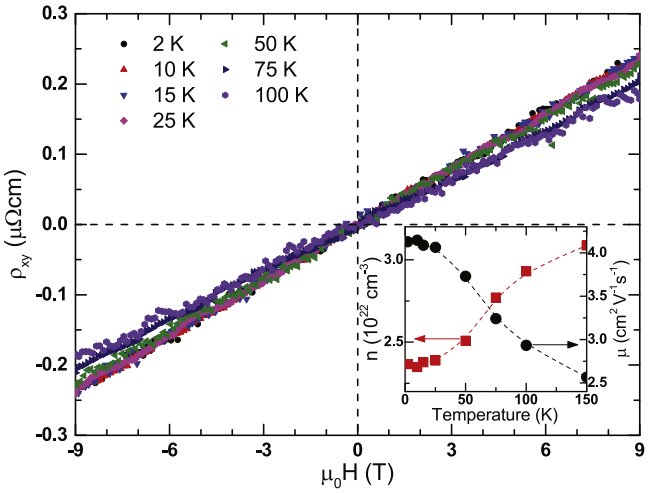

Figure 10. The isothermal magnetic field dependence of Hall resistivity ρ_{xy} with flowing current $I\|a$ and applying field $H\|c$ at selected temperatures between 2 and 150 K. The inset shows the temperature dependence of the carrier density and mobility estimated for single-crystal $HfAs_{1.67}Te_{0.12}$.

states. Based on the comparison with the BE of HfO_2 and HfN, we reasonably consider that two different valence states of Hf cation coexist in $HfAs_{1.67}Te_{0.12}$. The relative proportion can be roughly estimated as 0.63:0.37 by comparing the total areas corresponding state of Hf^{4+} and Hf^{3+}.

The spectra of Te and As measured on $HfAs_{01.67}Te_{0.12}$ single crystals are shown in figures 9(a) and (b), respectively. The two peaks observed in BE of Te shows a sharp doublet according to spin–orbit coupled final states of $3d_{5/2}$ and $3d_{3/2}$. The intensity ratio of $3d_{5/2}$: $3d_{3/2}$ in the fitting result is 1.4, which is in good agreement with the calculation $2J + 1$ with $J = 5/2$ and $3/2$. The BE corresponding to $3d_{5/2}$ and $3d_{3/2}$ is located at 572.6 and 583.0 eV, respectively, which agree well with the observed values of CdTe, GeTe and $Cu_{2-x}Te$ with a Te^{2-} state and a characteristic separation of 10.4 eV. The observation of spectra of Te 3*d* doublet shows another direct evidence of the presence Te in this ternary compound although the concentration is as small as 0.12. The As spectra clearly show two partially overlapped peaks at ~40.3 and ~41.6 eV, and another peak at 44.4 eV. The two peaks around 41 eV are close to the reported BE of 40.7 and 41.4 eV for the $3d_{5/2}$ and $3d_{3/2}$ in a standard GaAs with splitting energy of 0.7 eV. The higher BE peak at 44.4 eV is close to that of As binding observed in As_2O_3. Considering the structural characteristic obtained in single-crystal XRD analysis, we conclude that the different BEs of As are attributed to Hf–As and As–As bonds in $[Hf_2As_2]$ and [AsAs] layer, respectively.

Based on the analysis of XPS and single-crystal x-ray characterization, we propose a simple explanation for the valence state in $HfAs_{1.67}Te_{0.12}$. In PbFCl-type structure, As occupies two inequivalent sites, 2*b* and 2*c* site in As–As and Hf–As layer, respectively, as shown in figure 1. The As–As distance within the tetragonal As layer (the inset of figure 9) is 2.6 Å. Although this value is slightly longer than the typical As–As bond (2.4 Å), As charge of 1- from covalent As–As

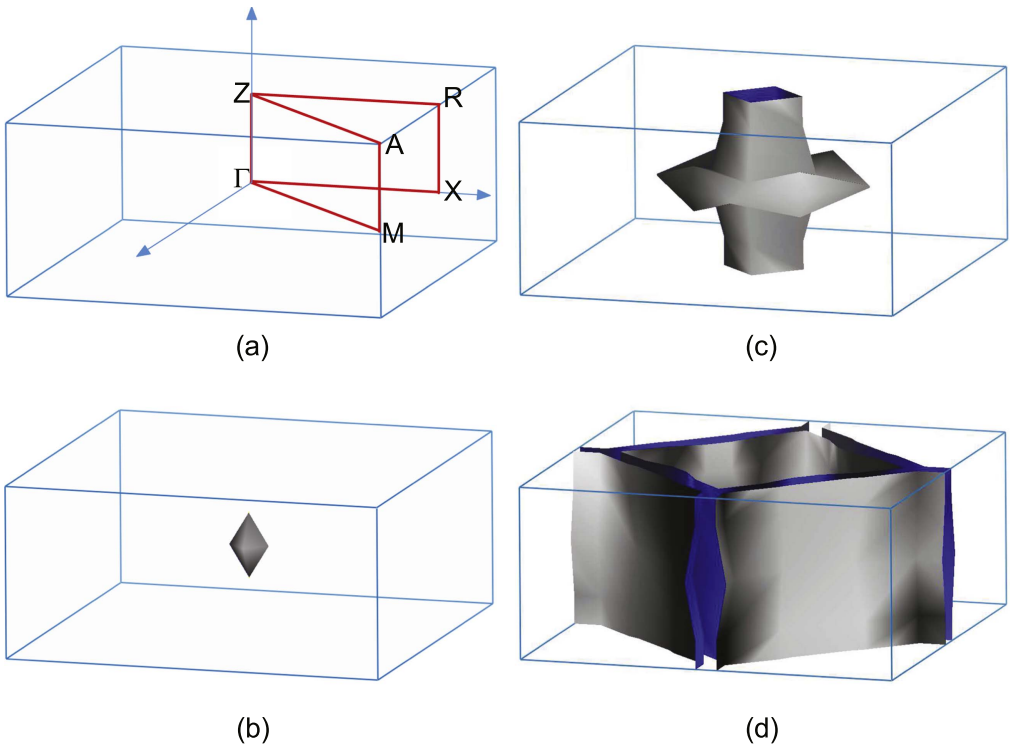

Figure 11. Reciprocal lattice (a), Fermi surfaces of band 13 (b), 14 (c) and 15 (d) of $HfAs_{1.67}Te_{0.12}$.

layer is estimated from the BE (figure 9) when compared with that of other As-containing compounds. Assuming a composition without vacancy, $HfAs_{2-x}Te_x$ has a valence state of $Hf^{4+}(As^{3-}_{1-x}Te^{2-}_{x})As^{1-}$, implying that the substitution of As^{3-} with Te^{2-} is kind of electron doping. On the other hand, single-crystal x-ray characterization suggests that the As/Te disorder prefers to occur in 2*c* site in Hf–As layer. Furthermore, it appears that As atoms form the tetragonal As–As layer after the full occupying at 2*c* site preferentially. In the present case of $HfAs_{1.67}Te_{0.12}$, near 0.21 vacancy per unit formula composition solely present within the As layers, as shown in $Hf(As_{0.88}Te_{0.12})As_{0.79}$. As already proved in the XPS (figure 8), Hf appears to be of 3+ and 4+ mixed-valence state. Thus, we reasonably consider that both the substitution of As with Te and the vacancies in As layers lead to a partial reduction effect to Hf^{4+}, e.g., $Hf^{4+}_{0.67}Hf^{3+}_{0.33}(As^{3-}_{0.88}Te^{2-}_{0.12})As^{1-}_{0.79}$ with valence balanced. Note that the proportion of Hf^{4+}:Hf^{3+} = 0.67:0.33 is in remarkable agreement with the estimated value (0.63:0.37) from the XPS for $HfAs_{1.67}Te_{0.12}$. Although such an approximation may overemphasize the charge transfer in complex solid-state structures, the scenario strongly supports the presence of mixed-valence state for Hf and As, which may play an important role in the appearance of superconductivity.

The carrier character in $HfAs_{1.67}Te_{0.12}$ is studied using Hall resistivity ρ_{xy}, which was measured with magnetic field $H\|c$ and current $I\|b$ at temperatures below 150 K. As shown in figure 10, $\rho_{xy}(H)$ shows a linear field dependence in field range of $|\mu_0 H| \leqslant 9$ T, and the slope varies weakly with increasing temperature from 2 to 150 K. Such a positive field effect in $\rho_{xy}(H)$ indicates that the hole-type carrier dominates the transport properties in the system, which is contrary to the electron carriers found in $ZrP_{2-x}Se_x$ [9]. The carrier density n and carrier mobility μ are obtained by simply fitting the linear $\rho_{xy}(H)$ with one-band model $n = 1/(eR_H)$ and $\mu = R_H/\rho_{xy}^{H=0}(T)$, where R_H represents the Hall coefficient that can be estimated by calculating the slope of $\rho_{xy}(H)$. As decreasing temperature, the n and μ show a monotonic increase and decrease, respectively, leading to the estimated carrier density and mobility in the order of 10^{22} cm^{-3} and $cm^2\ V^{-1}\ s^{-1}$ at low temperatures, as shown in the inset of figure 10.

Figure 11 shows Fermi surface (FS) topology. Three types of FSs (band 13–15) are observed. FS for bands 13 and 14 are three-dimensional, whereas that of 15 shows a two-dimensional-like feature. The FS topology is consistent with the weak anisotropy observed in SC phase. Furthermore, all three Fermi pockets are hole-type, which also supports the scenario of the hole-type carrier dominated transport properties. Figures 12(a) and (b) show the calculated band structure and density of state (DOS) character, respectively. By comparing the total and partial DOS, one can find that the contribution from Hf, tetragonal As layer and As/Te layer are comparable to each other, implying that a hybridized feature of *d* and *p* bands around Fermi level.

Upon comparison with other members in $APn_{2-x}Ch_x$ system (*A*: Zr, Hf; Pn: P, As; Ch: S, Se, Te) [6–9, 13] within PbFCl-type layered structure, we summarize some typical features observed on single-crystal $HfAs_{1.67}Te_{0.12}$ as follows. In the viewpoint of structure, the substitution of As with Te prefers to occur in Hf–As layer and the vacancies are present in tetragonal As–As layers, which are the common characters

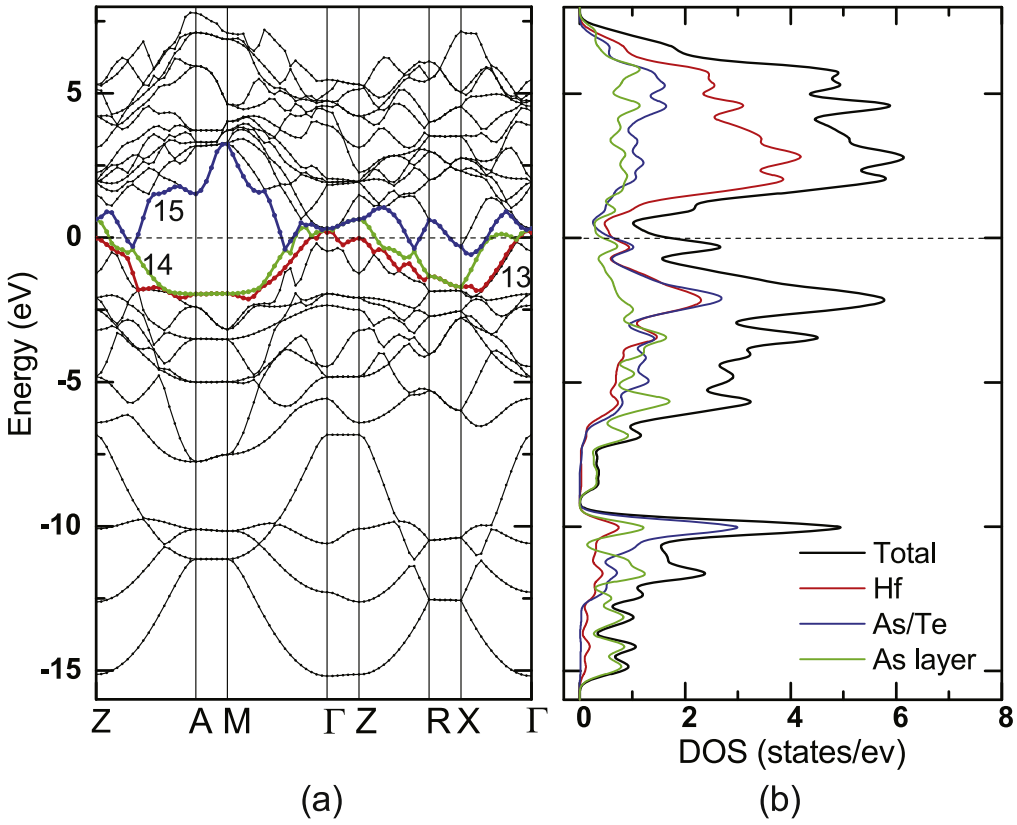

Figure 12. Band structure (a) and DOS profile (b) of $HfAs_{1.67}Te_{0.12}$.

of $APn_{2-x}Ch_x$ system. The substitution level ($x = 0.12$) is obviously much lower than the range limit $0.4 \leqslant x \leqslant 0.9$ observed in $ZrP_{2-x}Se_x$ [9]. The lattice parameters are expanded to $a = b \approx 3.7$ and $c \approx 8.1$ Å, which are near 0.05 and 0.2 Å larger than those of $ZrP_{2-x}Ch_x$ (Ch: S, Se) [8, 9], respectively. It is reasonably to consider that the change of the lattice parameters is caused by the slightly larger ion size of As as compared to P.

Secondly, the possible vacancy in the system was ignored in the studies on polycrystalline samples of $ZrP_{2-x}Ch_x$ (Ch: S, Se) [8, 9], whereas the vacancies have been confirmed in single-crystal analysis [13]. The vacancy estimated in the present system (0.21) is far away from the tie line $ZrAs_2$–$ZrSe_2$ on the As depleted side with the total concentration of As+Se between 1.90 and 1.99 [7]. The low T_c (0.14 K) of $ZrAs_{1.58}Se_{0.39}$ compared to the free-of-vacancies $ZrP_{1.54}S_{0.46}$ ($T_c = 3.7$ K) is considered to be related to the dynamical defects in the tetragonal As layers [13]. However, the opposite defect effect on T_c is confirmed in $HfAs_{2-x}Ch_x$ system. The superconductivity with $T_c = 0.52$ K observed in $HfAs_{1.7}Se_{0.2}$ [12] is apparently enhanced in $HfAs_{1.68}Te_{0.12}$ with $T_c = 1.67$ K. Although the different substitution level may also play a role in superconductivity, the correlation between vacancy and T_c can hardly be concluded as a simple mechanism compared to $ZrAs_{1.58}Se_{0.39}$ [13]. More efforts in the fields of theory and experiment are needed to clarify the SC mechanism.

Finally, the replacement of P and S by As and Se, respectively can hardly affect the transport properties including electrical resistivity and specific heat. $\rho(T)$ of single-crystal and polycrystalline samples show a considerably weak RRR that could be related to the substitution and vacancy effect. Although the electronic specific heat γ_n ($\sim$4 mJ mol^{-1} K^{-2}) is slightly enhanced as compared to 1.7 mJ mol^{-1} K^{-2}, the absolute value is still comparable to free electron system. In the meanwhile, a considerably weak increase is also present in $\rho(T)$ under high fields, as shown in figure 4. However, it is hard to discuss such a weak anomaly using a vacancy related orbital 2CK scenario as proposed for $ZrAs_{1.58}Se_{0.39}$ [13]. Furthermore, note that the C/T under fields (0.5 and 1 T) higher than the corresponding H_{c2} shows a clear upturn, might be related with a non-magnetic Kondo effect or field induced Schottky anomaly, which will be studied in more detail in a future study.

4. Conclusion

We succeeded in growing a PbFCl-type single crystal of $HfAs_{1.67}Te_{0.12}$ for the first time, which shows bulk superconductivity with $T_c = 1.67$ K that has been confirmed in $\rho(T)$, $\chi_{AC}(T)$ and $C/T(T)$. The results of single-crystal XRD analysis support the scenario that the substitution of As with Te prefers to occur in the Hf–As layer and the vacancies are present in the As–As layer. The experimental facts suggest that the superconductivity shows a conventional weak-coupling feature and is more likely three-dimensional. The XPS studies unfold the presence of the possible mixed-valence states of Hf and As. Both the Hall resistivity and the

electronic structure calculation imply that the hole-type carriers are dominant in the transport properties. The vacancy effect on T_c is rather different from that observed in $ZrAs_{1.58}Se_{0.39}$.

Acknowledgments

This work was supported by the National Key Research Program of China (Grant No. 2016YFA0401000, 2016YFA0300604), the Strategic Priority Research Program (B) of Chinese Academy of Sciences (Grant No. XDB07020100), and the National basic Research Program of China 973 Program (Grant No. 2015CB921303). We would like to thank Qinlin Guo for helpful discussions.

ORCID iDs

Shuai Zhang https://orcid.org/0000-0003-1342-7233

References

[1] Johnston D, Prakash H, Zachariasen W and Viswanathan R 1973 *Mater. Res. Bull.* **8** 777–84
[2] Morosan E, Zandbergen H W, Dennis B S, Bos J W G, Onose Y, Klimczuk T, Ramirez A P, Ong N P and Cava R J 2006 *Nat. Phys.* **21** 544–50
[3] Yamanaka S, Hotehama K and Kawaji H 1998 *Nature* **392** 580
[4] Taguchi Y, Hisakabe M and Iwasa Y 2005 *Phys. Rev. Lett.* **94** 217002
[5] Zhang S, Tanaka M and Yamanaka S 2012 *Phys. Rev.* B **86** 024516
[6] Schmidt M, Cichorek T, Niewa R, Schlechte A, Prots Y, Steglich F and Kniep R 2005 *J. Phys.: Condens. Matter* **17** 5481
[7] Schlechte A *et al* 2007 *Sci. Technol. Adv. Mater.* **8** 341–6
[8] Kitô H, Yanagi Y, Ishida S, Oka K, Gotoh Y, Fujihisa H, Yoshida Y, Iyo A and Eisaki H 2014 *J. Phys. Soc. Japan* **83** 074713
[9] Ishida S *et al* 2016 *Supercond. Sci. Technol.* **29** 055004
[10] Hulliger F 1964 *Nature* **204** 775
[11] Wilson J A and Yoffe A D 1969 *Adv. Phys.* **18** 193–335
[12] Czulucki A *et al* 2010 *Chem. Phys. Chem.* **11** 2639–44
[13] Cichorek T, Bochenek L, Schmidt M, Czulucki A, Auffermann G, Kniep R, Niewa R, Steglich F and Kirchner S 2016 *Phys. Rev. Lett.* **117** 106601
[14] Grosvenor A P, Cavell R G, Mar A and Blyth R I 2007 *J. Solid State Chem.* **180** 2670–81
[15] Maki K 1964 *Physics* **1** 127
[16] Maki K 1966 *Phys. Rev.* **148** 362–9
[17] Ginzburg V L and Landau L D 1950 *Zh. Eksp. Teor. Fiz.* **20** 1064
[18] Orlando T P, McNiff E J, Foner S and Beasley M R 1979 *Phys. Rev.* B **19** 4545–61